J. Fluid Mech. (1991), *vol.* 227, *pp.* 449–472
Printed in Great Britain

Blocking an inviscid shear flow

By MELVIN E. STERN
Department of Oceanography, Florida State University, Tallahassee, FL 32306, USA

(Received 12 September 1990 and in revised form 4 December 1990)

The upstream influence in an inviscid two-dimensional shear flow around a semi-circular 'cape' (radius A) is computed using a piecewise uniform vorticity model of a boundary-layer current. The area of this layer upstream from the cape increases as the square root of time t when A is small, and increases as t for larger A. Complete blocking occurs when A is approximately three times the boundary-layer thickness, in which case all oncoming particles accumulate in a large upstream vortex. The numerical results obtained from the contour dynamical method also show the generation of large eddies downstream from the obstacle.

1. Introduction

A familiar example of 'upstream influence' occurs in open channel flow when the controlling section is 'choked' so as to produce a Froude number exceeding unity, in which case the regime is changed by an upstream propagating surge wave. A weaker upstream influence occurs in a semi-infinite density stratified layer flowing with uniform velocity over an obstacle. For a review of the literature on these problems see Turner (1973). Hydraulic control can also occur in a rotating channel flow, the critical condition being determined by the propagation speed of Kelvin waves (Stern 1972). Whitehead, Leetma & Knox (1974) and Gill (1977) discuss the control by a strait of a shear flow with uniform potential vorticity, and generalizations are given by Stern (1975) and Pratt & Armi (1987). The topographic waves in a homogeneous fluid with a cross-stream variation in bottom depth provide another mechanism for hydraulic transitions and upstream influence. See Hughes (1986, 1987) for application to coastal currents.

The validity of the steady state and long-wave approximation used in these theories becomes doubtful if there is a flow reversal, and this is most likely to occur when an upstream shear current with vanishing wall velocity flows around an irregularity on the boundary. In this case the shorter waves and time dependence must be taken into account, and then the vorticity gradient can lead to a large disturbance propagating upstream. The effect will be demonstrated (§3) for the simplest case of inviscid two-dimensional flow around a semi-circular 'cape' (figure 2). (We remark that such flows are realizable in a rotating fluid because three-dimensional turbulence is suppressed, and relative vorticity tends to be conserved.)

Before turning to this main calculation, some helpful insights will be obtained (§2) using a nonlinear long-wave theory, and the simple results will suggest the flow reversal effect to be investigated by a more complete theory.

A solution of the Euler equations is necessary for this purpose, and the relatively simple geometry in figure 2 will be used. Here we have a semi-infinite fluid bounded by a wall with a semi-circular 'cape' of radius A. Upstream from this there is a piecewise uniform vorticity flow of the boundary-layer type. The temporal evolution

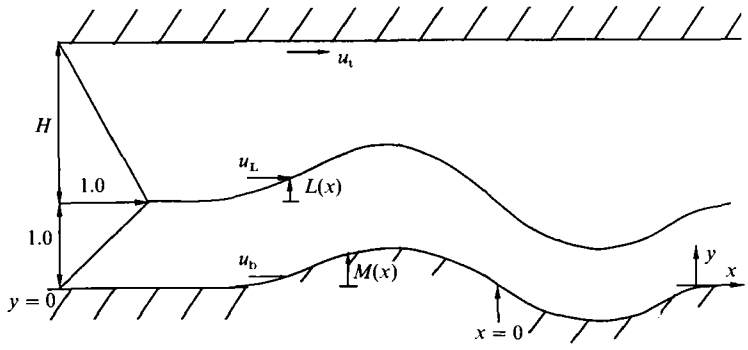

FIGURE 1. Schematic diagram of a laminar upstream jet flowing in a channel whose total width varies slowly in the downstream direction. $L(x)$ is the steady-state displacement of the interface separating the piecewise uniform vorticity layers, and $u_L(x)$ is the downstream velocity. The wall velocities are $u_b(x)$, $u_t(x)$.

of the interface separating the vortical domains will be computed using the well-known contour dynamical method, due consideration being given to the irregular boundary condition.

This obstacle 'trips' the boundary layer, producing aperiodic disturbances extending far downstream as well as upstream. It is therefore necessary (and maybe desirable) to focus attention mainly on one aspect of these complex effects, viz. the fraction of oncoming boundary-layer fluid which is prevented from passing around the cape. It will be shown that when the cape radius exceeds the boundary-layer thickness, the fluid in this layer accumulates in an upstream eddy. The size of this is much larger than the upstream vortex which forms in a *uniform* vorticity flow having either zero viscosity or very large viscosity (Higdon 1985).

2. Long-wave theory

2.1. *A piecewise vorticity jet in a channel of slowly varying width*

At $x=-\infty$ in figure 1 the non-dimensional vorticity is -1 for $y<1$, and $1/H$ for $1\leqslant y\leqslant H+1$. The non-dimensional basic velocity profile satisfies $\bar{u}(1)=1$, $\bar{u}(0)=0$ and $\bar{u}(1+H)=0$. The undisturbed laminar jet approaches a section centred around $x=0$ where the wall displacement $y_b(x)=M(x)$ varies slowly with x, and we assume a steady and slowly varying downstream velocity field $u(x,y)\geqslant 0$. Let $u_L(x)=u(x, 1+L)$ denote the velocity on the interface ($y=1+L(x)$) separating the piecewise uniform vorticity layers, and let $u_b=u(x,M(x))$, $u_t=u(x,1+H)$. According to the long-wave approximation, the vorticity is $-\partial u/\partial y$, and integration across the stream gives

$$u_L=u_b+1+L-M, \tag{2.1}$$

$$u_L=u_t+(H-L)/H. \tag{2.2}$$

The continuity of mass flux for each layer requires

$$(u_L+u_b)(1+L-M)=1, \tag{2.3}$$

$$(u_L+u_t)(H-L)=H. \tag{2.4}$$

Equations (2.1) and (2.2) are used to eliminate u_b, u_t from the last two equations, and then the elimination of $2u_L$ gives the following implicit equation for $L(x)$:

$$\xi+1/\xi-(\lambda+1/\lambda)=0, \tag{2.5}$$

where
$$\xi \equiv 1+L-M, \tag{2.6a}$$
$$\lambda \equiv 1-L/H. \tag{2.6b}$$

The two ($\pm$) solutions for ξ in (2.5) are
$$(\xi) = \begin{pmatrix} 1/\lambda_+ \\ \lambda_- \end{pmatrix} \tag{2.7}$$
and from (2.6*a*, *b*) another equation for ξ is
$$\xi = 1-M-H(\lambda-1). \tag{2.8}$$
Elimination of ξ then gives the two solutions
$$-M = H(\lambda_\pm - 1) - 1 + \begin{pmatrix} 1/\lambda_+ \\ \lambda_- \end{pmatrix} \tag{2.9}$$
at each $M(x)$. When either λ_+ or λ_- equals unity, $M = 0$, and therefore $\xi = 1$ and $L_\pm = 0$. Each of the two solutions of (2.9) start at $x = -\infty$ (where $M = 0$) and continue to larger x. Which, if any, of these steady long-wave solutions is a valid approximation to the more complete equations of motion? In connection with this question, it will now be shown that if $M(x)$ vanishes at $x = 0$ and if $\mathrm{d}M(0)/\mathrm{d}x \neq 0$ (as in figure 1) then *both* solutions have a flow reversal at $x = 0$.

The wall velocity obtained from (2.1), (2.3) and (2.6*a*) is $u_b = \frac{1}{2}(1/\xi - \xi)$, and therefore $u_b = 0$ and $\mathrm{d}u_b/\mathrm{d}\xi = -1$ at the point $\xi = 1$, which corresponds to $M(0) = 0$. From (2.7), (2.8) we then obtain $\mathrm{d}M(1)/\mathrm{d}\xi = -1 \pm H$, and it follows that $\mathrm{d}u_b/\mathrm{d}M = (\mathrm{d}u_b/\mathrm{d}\xi)(\mathrm{d}M/\mathrm{d}\xi)^{-1} = -(1 \pm H)^{-1}$ at $x = 0$. For $H \neq 1$ this shows that a flow reversal $u_b < 0$ occurs on one side or the other of $x = 0$, and an isolated eddy with closed streamlines is implied. But the validity of this must be doubted because of the long-wave and steady-state assumptions.

2.2. *Temporal evolution of long waves*

Further insight may be obtained by relaxing the steady assumption and by considering the initial-value problem for a large $L(x,t)$ disturbance in a *uniform* channel (i.e. set $M(x) \equiv 0$ in figure 1). At $x = \pm\infty$ in the undisturbed jet the total transport between the walls is $\frac{1}{2}(1+H)$, and since this must equal the total transport at any x in the disturbed region is follows that
$$(u_L + u_b)(1+L) + (u_L + u_t)(H - L(x,t)) = H+1. \tag{2.10}$$
When $M = 0$, (2.1)–(2.2) are still applicable and elimination of (u_b, u_t) in the above relation gives
$$2u_L = 1 + \frac{(1+L)^2 + (H-L)^2/H}{H+1}. \tag{2.11}$$
In the $0 < y < L$ layer the conservation of mass requires
$$\frac{\partial L}{\partial t} + \frac{\partial}{\partial x}(\tfrac{1}{2}(u_L + u_b)(1+L)) = 0,$$
and by using (2.1), (2.2) we get
$$\frac{\partial L}{\partial t} + \frac{1}{2}\frac{\partial}{\partial x}((1+L)(2u_L - 1 - L)) = 0.$$

When (2.11) is introduced this reduces to the hyperbolic equation

$$\frac{\partial L}{\partial t}+c(L)\frac{\partial L}{\partial x}=0,$$

where the propagation speed

$$c(L)=-L(1-1/H)+\tfrac{3}{2}L^2/H \tag{2.12}$$

is negative for sufficiently large H and for $L(x,0)>0$. Under the latter conditions (2.11) gives $u_L\to 1$, and (2.1) gives $u_b<0$. Since this flow reversal is imposed initially, no logical objection can be made to its subsequent presence in the long-wave theory, and this shows that the reversal will propagate upstream with the large L-ridge. Of course the continual steepening of the wavefront causes the long-wave theory to fail, and then the complete Euler equations must be used. Despite these reservations the suggestion is that the flow forced by the obstacle (figure 1) might lead to a flow reversal which propagates upstream into a region where the wall is flat.

It is worth demonstrating that the result of this subsection is not an artifact of the piecewise uniform vorticity model, but it also occurs for long-wave disturbances in a jet whose vorticity $\zeta\approx-\partial u/\partial y$ increases *smoothly* from $y=0$ to $y=H+1\equiv\bar{H}$. This vorticity relation gives

$$\int_0^{\bar{H}}(\bar{H}-y)\,\zeta\,\mathrm{d}y=\bar{H}u(x,0,t)-\int_0^{\bar{H}}u\,\mathrm{d}y.$$

Since the last term is independent of x, the difference (Δ) in wall velocities at any two sections (x) is given by

$$\bar{H}\,\Delta u(x,0,t)=\Delta\int_0^{\bar{H}}(\bar{H}-y)\,\zeta(x,y,t)\,\mathrm{d}y. \tag{2.13}$$

Consider an initial condition in which each vorticity isopleth (except those at $y=0,\bar{H}$) *increases* its ordinate (y) monotonically with x, from one constant y-value at $x=-\infty$ to a larger constant value at $x=+\infty$ (with the sloping part of the isopleths centred at $x=0$). Then on a line of constant y, the value of ζ at a downstream x is less than the upstream value at $x=-\infty$, and therefore the right-hand side of (2.13) is negative. Since the wall velocities of the jet at $x=-\infty$ are assumed to vanish, it follows that negative u occur near $x=0, y=0$. Furthermore, the downstream pressure gradient is negligible in the long-wave approximation, and each parcel conserves its x-momentum (Stern & Paldor 1983). Therefore the maximum upstream u on $y=0$ is conserved and propagated upstream with its own velocity. This effect is similar to that which occurs in the piecewise uniform vorticity model.

2.3. *Upstream propagation in a boundary-layer flow*

We also want to show that a similar effect occurs for a boundary-layer flow like that in figure 2 when the obstacle is removed ($A=0$). This piecewise uniform vorticity flow has a non-dimensional velocity profile $\bar{u}(y)$ such that $\bar{u}(0)=0$, $\bar{u}(y)=y$ for $0\leqslant y\leqslant 1$, and $\bar{u}(y)=1-(y-1)\zeta_2$ for $\infty>y\geqslant 1$, where $0\geqslant\zeta_2>-1$. Further downstream the vorticity interface is initially displaced from $y=1$ by an amount which varies slowly with x. In a coordinate system moving downstream with velocity $+1$, let $u_b(x,t)$ denote the wall velocity, and $u_L(x,t)$ the interfacial velocity. At any point above the interface, the conservation of mass [in $\infty>y>1+L(x,t)$] requires that $u(x,y,t)=u(-\infty,y,t)$, and $\partial u/\partial y=-\zeta_2$ requires $u_L(x,t)=-\zeta_2 L(x,t)$. In the lower

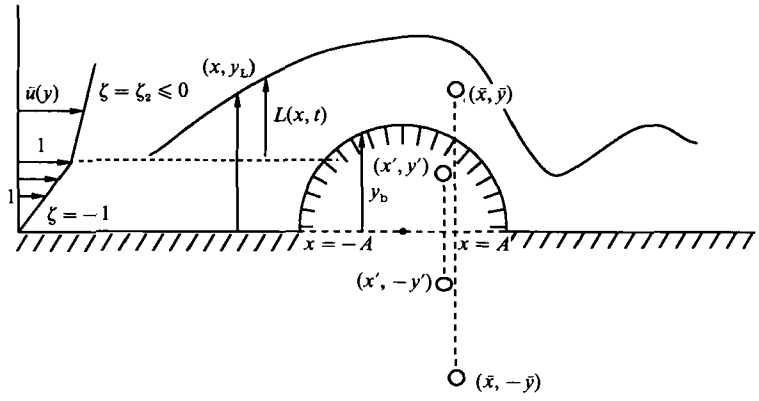

FIGURE 2. Schematic diagram of a piecewise uniform vorticity flow around a semi-circular cape. The displacement of the interface separating the two uniform vorticity domains is $L(x,t) = y_L(x, t)-1$. A small circular element of vorticity at $(\bar{x}, \bar{y})$ is shown, together with the three images necessary to satisfy the boundary conditions on all rigid surfaces.

layer, the vorticity (-1) requires $u_b = u_L-(1+L)$, and the conservation of mass requires

$$0 = \frac{\partial L}{\partial t}+\frac{1}{2}\frac{\partial}{\partial x}(u_L+u_b)(1+L) = \frac{\partial L}{\partial t}-\frac{1}{2}\frac{\partial}{\partial x}((2\zeta_2 L+1+L)(1+L)).$$

Therefore $\partial L/\partial t+c_1(L)\,\partial L/\partial x = 0$, where the propagation speed in the moving coordinate system is $c_1 = -(1+L)-\zeta_2(1+2L)$, and in the original coordinate system (stationary with respect to the wall) the propagation speed is

$$c(L) = -L-\zeta_2(1+2L). \tag{2.14}$$

For $\zeta_2 = 0$ all finite-amplitude elevation waves propagate upstream ($c < 0$), and this also holds for small negative ζ_2 provided L is sufficiently large. If $\zeta_2 < 0$, the *necessary* condition for an upstream propagation is

$$-\zeta_2 < \frac{L}{1+2L} < \tfrac{1}{2} \tag{2.15}$$

for some $L > 0$.

In a *forced* flow problem (§3), such as may be produced by inserting an obstacle (figure 2) with large A, the maximum interfacial displacement L should be (§3) of order $A-1$, and (2.15) suggests

$$-\zeta_2 \sim \frac{A-1}{1+2(A-1)} \tag{2.16}$$

as an estimate of the critical condition for a large amplitude upstream influence and a large blocking effect. We shall refer to this in §6.4.

3. Contour dynamical equations for boundary-layer flow around a semi-circular cape

We turn to the main problem (figure 2). The laminar velocity at $x = -\infty$ is again given by

$$\bar{u}(y) = \begin{Bmatrix} y & \text{for } y \leqslant 1 \\ 1-\zeta_2(y-1) & \text{for } y \geqslant 1 \end{Bmatrix}, \tag{3.1}$$

where the lengthscale used in the non-dimensionalization is the upstream boundary-layer thickness and the timescale is the reciprocal vorticity of this layer. Then A denotes the non-dimensional cape radius, and $L(x,t) = y_L(x,t) - 1$ is the displacement of the interface above a $y = 1$ datum level. This will intersect the cape if $A > 1$, in which case another datum level

$$y_b(x) = \max(1, (A^2 - x^2)^{\frac{1}{2}}), \tag{3.2}$$

will be needed.

The total velocity $V(x,y,t)$ is conveniently divided into three parts:

$$V = V_s + V_0 + V_c, \tag{3.3}$$

where

$$V_s \equiv \{\bar{u}(y), 0\} + V_A \tag{3.4}$$

is the sum of the undisturbed horizontal velocity (3.1) and an *irrotational* field $V_A(x,y)$ which makes the normal component of (3.4) vanish on all rigid boundaries. The V_s field contributes an amount (-1) to the vorticity in the fluid region between $y = 1$ and the solid boundary, and ζ_2 is the contribution beyond $y = 1$. The total fluid vorticity, however, will deviate from these values in those areas lying between the disturbed interface ($L(x,t)$) and the datum level (3.2). Therefore the velocity $V_0 + V_c$ produced by these 'vorticity anomalies' must be added to V_s. For example, at $\bar{x}, \bar{y}$ in figure 2 $L(\bar{x},\bar{y}) > 0$, the total vorticity is (-1), the undisturbed vorticity is ζ_2, and therefore the vorticity anomaly is $(-1-\zeta_2)$. The velocity field induced by all such elements in the presence of the boundary must be summed.

An area element of vorticity anomaly $\hat{\zeta}$ at $(\bar{x},\bar{y})$ would, in the absence of all boundaries, produce a streamfunction $(4\pi)^{-1}\,\mathrm{d}\bar{x}\,\mathrm{d}\bar{y}\,\hat{\zeta}[\ln(x-\bar{x})^2 + (y-\bar{y})^2]$ at point (x,y). To satisfy the boundary conditions in figure 2 we add an image vortex relative to a (full) circle, and two additional image vortices relative to the symmetry plane ($y = 0$). The first of the three images is located at the 'inverse' point (x',y') of $(\bar{x},\bar{y})$, and the two latter images are at $(x', -y')$ and $(\bar{x}, -\bar{y})$, respectively. The sum of these four point vortices (with appropriate signs) gives the contribution to the streamfunction of each vortex anomaly, and integration over $(\bar{x},\bar{y})$ gives the total streamfunction for $V_0 + V_c$. These four Green functions are conveniently re-grouped into two components, one of which is the sum of $(\bar{x},\bar{y})$ and its $(\bar{x}, -\bar{y})$ image (figure 2), this component being denoted by V_0 and by its associated streamfunction ψ_0. The influence of the inverse point at

$$\left.\begin{aligned} x' &= A^2\bar{x}/(\bar{x}^2 + \bar{y}^2), \\ y' &= A^2\bar{y}/(\bar{x}^2 + \bar{y}^2), \end{aligned}\right\} \tag{3.5}$$

and its image $(x', -y')$ is combined in the second component (ψ_c, V_c).

As previously mentioned, the vorticity anomaly is $\hat{\zeta} = -1-\zeta_2$ if $\bar{y} > y_b$, and if $\bar{y} < y_b$ then $\hat{\zeta} = 1+\zeta_2$. Consider first the case where $L(x,t)$ is a single-valued function of x. Then the contribution to the streamfunctions of all the anomalies in the interval $\mathrm{d}\bar{x}$ requires an integration (of the Green functions) from $\bar{y} = y_b(\bar{x})$ to $\bar{y} = y_L(\bar{x})$ if $y_L > y_b$, and if $y_L < y_b$ the integration goes from y_L to y_b. Because of the changed sign of $\hat{\zeta}$ in these two cases it follows that for both

$$\psi_0 = \frac{(-1-\zeta_2)}{4\pi}\int_{-\infty}^{+\infty}\mathrm{d}\bar{x}\int_{y_b}^{y_L}\mathrm{d}\bar{y}\ln\left[\frac{(x-\bar{x})^2 + (y-\bar{y})^2}{(x-\bar{x})^2 + (y+\bar{y})}\right],$$

$$V_0 = (v_0, u_0) = (\partial\psi_0/\partial x, -\partial\psi_0/\partial y).$$

Similar considerations for the inverse point and its image give

$$\psi_c = \frac{(1+\zeta_2)}{4\pi}\int_{-\infty}^{+\infty} d\bar{x}\int_{y_b}^{y_L} d\bar{y}\ln\frac{(x-x')^2+(y-y')^2}{(x-x')^2+(y+y')^2},$$

$$V_c = (v_c, u_c) = (\partial\psi_c/\partial x, -\partial\psi_c/\partial y).$$

It may be shown that if the interface is a multi-valued function of x the same relations hold, provided the $d\bar{x}$ integration is performed along each line element of the contour. Although the computation of (u_0, v_0) may be reduced by means of Green's Theorem to *single* integrals along the $L(x,t)$ contour, and along $y_b(x)$, the computation of $V_c = (u_c, v_c)$ requires an explicit cross-stream integration as well as a downstream contour integration.

For the simpler case $A < 1$, the datum level is $y_b = 1$ everywhere. When the velocities obtained from ψ_0 (with the aid of Green's Theorem) are evaluated on the contour the result is

$$\frac{v_0(x, L(x,t)\,t)}{(-1-\zeta_2)} = \frac{1}{4\pi}\int_{-\infty}^{+\infty} dL(\bar{x})\ln\left[\frac{(x-\bar{x})^2+(L(x)-L(\bar{x}))^2}{(x-\bar{x})^2+(L(x)+L(\bar{x})+2)^2}\right], \tag{3.6}$$

$$\frac{u_0(x,L,t)}{(-1-\zeta_2)} = \frac{1}{4\pi}\int_{-\infty}^{+\infty} d\bar{x}\ln\left[\frac{(x-\bar{x})^2+(L(x)-L(\bar{x}))^2}{(x-\bar{x})^2+L^2(x)}\,\frac{(x-\bar{x})^2+(L(x)+L(\bar{x})^2+2)^2}{(x-\bar{x})^2+(L(x)+2)^2}\right]. \tag{3.7}$$

The interfacial velocities obtained from ψ_c are

$$\frac{v_c(x,L,t)}{(-1-\zeta_2)} = -\frac{1}{2\pi}\int_{-\infty}^{+\infty} d\bar{x}\int_{1}^{L(\bar{x})+1}(d\bar{y})(x-x')$$
$$\times\left[\frac{1}{(x-x')^2+(1+L(x)-y'(\bar{x}))^2}-\frac{1}{(x-x'(\bar{x}))^2+(1+L(x)+y'(\bar{x}))^2}\right], \tag{3.8}$$

$$\frac{u_c(x,L,t)}{(-1-\zeta_2)} = +\frac{1}{2\pi}\int_{-\infty}^{+\infty} d\bar{x}\int_{1}^{1+L(\bar{x})} d\bar{y}$$
$$\times\left[\frac{1+L(x)-y'(\bar{x},\bar{y})}{(x-x')^2+(1+L(x)-y')^2}-\frac{1+L(x)+y'}{(x-x')^2+(1+L(x)+y')^2}\right], \tag{3.9}$$

and all $\bar{x}$ integrations are taken along the $L(x,t)$ contour.

The irrotational part V_A of (3.4) was computed from a streamfunction $\psi_A(r,\theta)$, using polar coordinates (r,θ). Since the normal component of V_A on the cape must be equal and opposite to $\cos\theta\bar{u}(y) \equiv A\cos\theta\sin\theta$, we obtain $\psi_A(A,\theta) = \frac{1}{4}A^2(1-\cos 2\theta)$ as a boundary condition, and $\psi_A(r,0) = \psi_A(r,\pi) = 0$ for $r \geqslant A$ must also be satisfied in the solution of Laplace's equation. For this solution we used a Fourier sine series

$$\psi_A(r,\theta) = -\frac{4A^2}{\pi}\sum_{m=1}^{\infty}\left(\frac{A}{r}\right)^{2m-1}\frac{\sin(2m-1)\theta}{(2m-1)[(2m-1)^2-4]}. \tag{3.10}$$

Then the Cartesian components of the velocity field were added to the undisturbed $\bar{u}(L)$ to get

$$v_s(x, L(x,t), t) = \frac{4A}{\pi}\sum_{m=1}^{\infty}\left(\frac{A}{r}\right)^{2m}\frac{\sin(2m\theta)}{(2m-1)^2-4}, \tag{3.11a}$$

$$u_s(x,L,t) = \frac{4A}{\pi}\sum_{m=1}^{\infty}\left(\frac{A}{r}\right)^{2m}\frac{\cos(2m\theta)}{(2m-1)^2-4}+\begin{cases}1+L(x,t) & \text{if } L<0,\\ 1-\zeta_2 L & \text{if } L>0,\end{cases} \tag{3.11b}$$

$$r^2 = x^2+y_L^2,$$
$$\theta = \arcsin(y_L/r). \tag{3.11c}$$

For use in §6.2 we note that when $A \to 0$ and $y_L \to 1$, the leading term in (3.11*a*), or

$$v_s(x, y = 1) = -\frac{8A^3}{3\pi}\frac{x}{(x^2+1)^2} \tag{3.12}$$

gives the asymptotic value of the interfacial velocity forced by the cape.

When $A > 1$ (figure 2), $y_b(x)$ exceeds unity over a portion of the cape, the foregoing formula must be modified by changing the lower limit of the $\bar{y}$ integration in (3.8)–(3.9) to $y_b(\bar{x})$ (equation (3.2)). Additionally, in the denominators of (3.7) the term $L^2(x)$ must be replaced by $(L(x)+1-y_b)^2$, and the term $(L(x)+2)^2$ must be replaced by $(L(x)+1+y_b(\bar{x}))^2$. Since no fluid exists in the segment $|x| \leqslant x_0 = (A^2-1)^{\frac{1}{2}}$ of the cape intercepted by $y_b = 1$, (3.6) gives rise to an extraneous contribution

$$\frac{(-1-\zeta_2)}{4\pi}\int_{-x_0}^{x_0} dx_b \left(\frac{dy_b}{dx_b}\right) \ln \frac{(x-x_b)^2+(1+L(x)-y_b(x_b))^2}{(x-x_b)^2+(1+L(x)+y_b(x_b))^2}$$

to v_0, and therefore this contribution was subtracted from (3.6). The Fourier series solutions corresponding to (3.11*a*, *b*) must also be changed to

$$v_s = -(1+\zeta_2)A\sum_1^\infty (2m-1)\beta_m (A/r)^{2m}\sin(2m\theta), \tag{3.13a}$$

$$u_s = -(1+\zeta_2)A\sum_1^\infty (2m-1)\beta_m (A/r)^{2m}\cos(2m\theta) + \bar{u}(L), \tag{3.13b}$$

$$\tfrac{1}{2}\pi\beta_m = -\sin\theta_c \begin{cases} \theta_c - \tfrac{1}{2}\pi & \text{if } m = 1 \\ \dfrac{\sin 2(m-1)\theta_c}{2m-1} & \text{if } m \neq 1 \end{cases}$$

$$-\sin\theta_c\left[-\frac{\sin 2m\theta_c}{2m}+\frac{2}{2m-1}\sin\theta_c\cos(2m-1)\theta_c\right]$$

$$+\frac{1}{4}\left[\frac{\cos(2m+1)\theta_c}{2m+1}+\frac{\cos(2m-3)\theta_c}{2m-3}-\frac{2}{2m-1}\cos 2\theta_c\cos(2m-1)\theta_c\right],$$

$$\theta_c = \sin^{-1}(1/A).$$

4. Limiting cases

4.1. $\zeta_2 \to (-1)$

This uniform vorticity flow corresponds to an elementary problem in potential theory, in which there are no anomalies ($V_0 = 0 = V_c$) in the flow around the obstacle. A simple steady state exists in which $L(x)$ merely denotes the deflection of a streamline originating at $(-\infty, 1)$. An expression for $L(x)$ in polar coordinates $(r_0(\theta))$ is obtained by setting the constant value of the streamfunction $\frac{1}{2}\psi_A(r,\theta) - y^2 = \psi_A(r_0, \theta) - \frac{1}{2}r_0^2\sin^2\theta$ equal to $-\frac{1}{2}$, and (3.10) then gives an equation

$$-\frac{8}{\pi}\sum_{\substack{n=1\\ \text{odd}}}^{\infty}\left(\frac{A}{r_0}\right)^n \frac{\sin(n\theta)}{n(4-n^2)} + \left(\frac{r_0(\theta)}{A}\right)^2 \sin^2\theta = \frac{1}{A^2} \tag{4.1}$$

whose roots $r_0(\theta)$ were obtained numerically.

The question then arises as to whether there exists a neighbouring steady solution for the interface when ζ_2 is slightly greater than (-1), in which case a first-order

differential equation, $v = \mathrm{d}L/\mathrm{d}t = u\,\partial L/\partial x$, has to be satisfied subject to *two* boundary conditions ($L(-\infty) = 0$, $\partial L(+\infty)/\partial x = 0$). By perturbing $u\,\partial L/\partial x - v = 0$ relative to (4.1) a linear first-order equation was obtained, and a solution was shown to exist due to the fact that the leading-order term (from (4.1)) for v_s is an antisymmetric function of x, and u_s is a symmetric function. This establishes one region ($\zeta_2 \to -1$) of the parametric space (A, ζ_2) in which there is a *steady* state.

4.2. $A \to 0$ *for any fixed* $\zeta_2 < 0$

In this case (3.12) and its (half-range) Fourier transform,

$$v_s = \frac{4A^3}{3\pi}\,\mathrm{Re}\int_0^\infty \mathrm{d}k\,\mathrm{e}^{\mathrm{i}kx}\,\mathrm{e}^{-k}\,\mathrm{i}k, \tag{4.2}$$

have small amplitude, and therefore the linearized equation $v_s + v_0 = \partial L/\partial t + \partial L/\partial x$ may be used to compute the small $L(x,t)$. Note that no v_c component appears here because the equal and opposite vortices at (x', y') and $(x', -y')$ in figure 2 are very close to each other at $x = 0$, $y = 0$ when $A \to 0$, and thus their dipole field on $y = 1$ is negligible.

The calculation for this forced linear problem is facilitated by noting that the functional relation (3.6) between v_0 and L must reduce to the same form as that which occurs in the corresponding *free* wave evolutionary problem when $A = 0$. Therefore when $\partial L/\partial t + (\partial L/\partial x - v_0) = v_s$ is Fourier transformed using

$$L(x,t) = \mathrm{Re}\int_0^\infty \mathrm{d}k\,\mathrm{e}^{\mathrm{i}kx}\,\hat{L}(k,t) \tag{4.3}$$

and (4.2), we obtain the forced wave equation

$$\frac{\partial \hat{L}}{\partial t} + \mathrm{i}kc(k)\,\hat{L} = \frac{4A^3}{3\pi}\,\mathrm{i}k\,\mathrm{e}^{-k}, \tag{4.4}$$

where

$$c(k) = 1 - (1+\zeta_2)\frac{(1-\mathrm{e}^{-2k})}{2k} \tag{4.5}$$

is the propagation speed of the aforementioned free waves (Stern & Pratt 1985). For an initial condition $L(x,0) = 0$ the solution of (4.3)–(4.4) is

$$\left(\frac{4A^3}{3\pi}\right)^{-1} L(x,t) = \mathrm{Re}\int_0^\infty \mathrm{d}k\,\mathrm{e}^{\mathrm{i}kx}[1-\mathrm{e}^{-\mathrm{i}kc(k)t}]\,\mathrm{e}^{-k}/c(k). \tag{4.6}$$

When ζ_2 is negative definite, $c(k)$ is positive definite, and the steady-state solution at finite x is obtained from (4.6) by discarding the term containing t. Of particular interest is the area

$$\mathrm{UPAREA} \equiv \int_{-\infty}^0 L\,\mathrm{d}x, \tag{4.7}$$

bounded by L upstream from the cape, and this is readily found to be

$$\mathrm{UPAREA} = \frac{2A^3}{3(-\zeta_2)} \quad \text{for } -\zeta_2 \to 0^+.$$

4.3. $\zeta_2 = 0, A \to 0$

For the singular case $\zeta_2 = 0$ the asymptotic value of L for $t \to \infty$, $x \leqslant 0$ can be

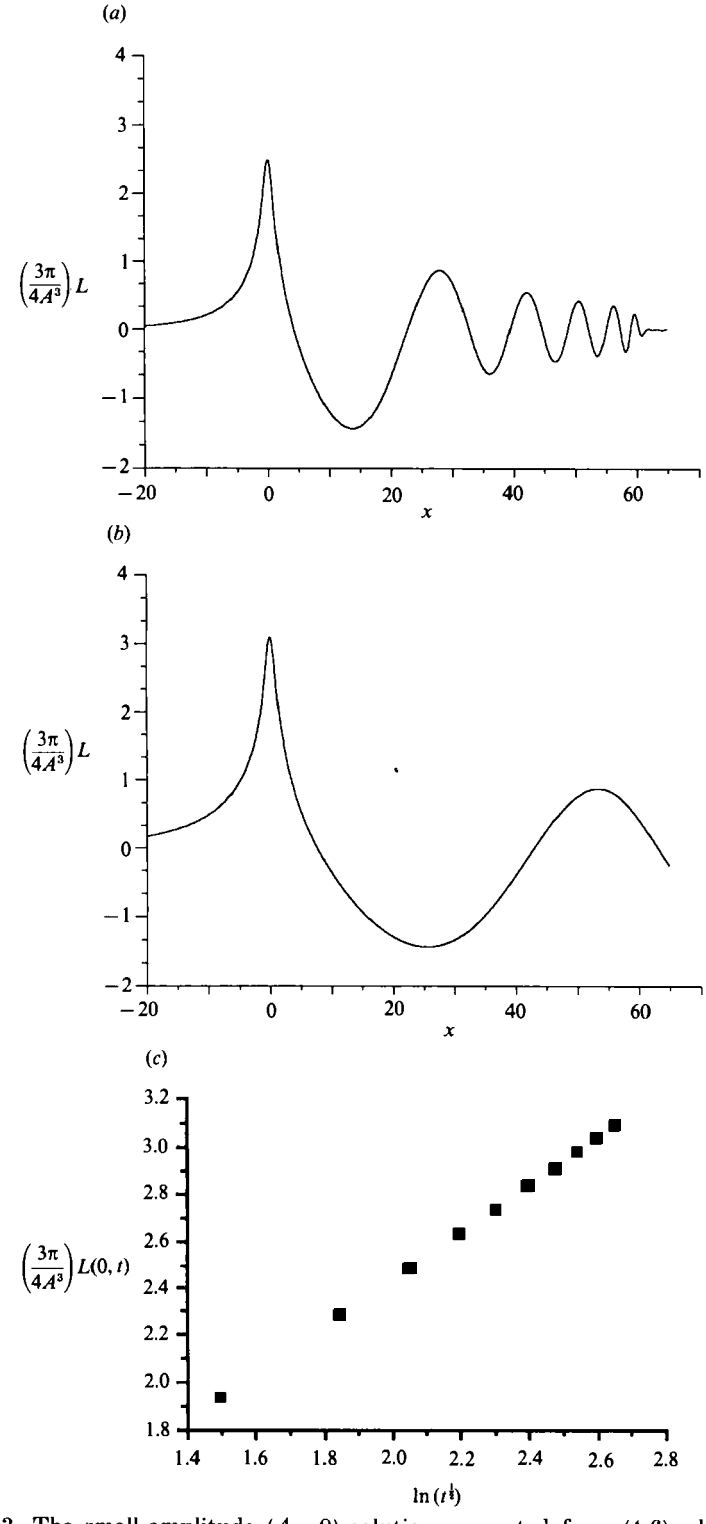

FIGURE 3. The small-amplitude ($A \to 0$) solution computed from (4.6) when $\zeta_2 = 0$. (*a*) $t = 60$; (*b*) $t = 200$; (*c*) maximum L as a function of $\ln t^{\frac{1}{2}}$. The points lie on a line whose ordinate is $0.998 \ln t^{\frac{1}{2}} + 0.443$.

computed by expanding $c = k - \frac{4}{6}k^2 + \ldots$, and substituting this in (4.6). By setting $k^2 = 1/t$ and by discarding terms of order $1/t^{\frac{1}{2}}$ in c we then get

$$\left(\frac{4A^3}{3\pi}\right)^{-1} L(0,t) \approx \mathrm{Re}\int_0^\infty \frac{\mathrm{d}z}{z}(1-\exp(-\mathrm{i}z^2))\exp(-zt^{-\frac{1}{2}}).$$

When this integral is broken into two segments, the first going from $z = 0$ to $z = 1$ (say), and the second going from $z = 1$ to $z = \infty$, then it is easy to show that the former is negligible as $t \to \infty$, and the latter gives the asymptotic value

$$\lim_{t\to\infty}\left(\frac{4A^3}{3\pi}\right)^{-1} L(0,t) = \ln t^{\frac{1}{2}}. \tag{4.8}$$

By integrating (4.6) and then taking the t-limit it can also be shown that

$$\lim\left(\frac{4A^3}{3\pi}\right)^{-1} \int_{-\infty}^{0} L(x,t)\,\mathrm{d}x = \tfrac{1}{2}(\tfrac{1}{2}\pi)^{\frac{1}{2}}(\tfrac{1}{2}t)^{\frac{1}{2}}. \tag{4.9}$$

The plots of $L(x,t) = 0$ in figure 3 were obtained from the more accurate integral (4.6), and the best fitting straight line to figure 3(*c*), $L(0,t) = 0.998\ln t^{\frac{1}{2}} + 0.443$, has a slope agreeing with the asymptotic value in (4.8). This calculation shows that a slow ($t^{-\frac{1}{2}}$) rate increase in the area of the upstream boundary layer occurs for $A \to 0$ when $\zeta_2 = 0$. The increase is compensated by an increase in the negative area of the downstream trough (figure 3*b*).

5. Numerical calculation for $A \leqslant 1$

The implementation of the formulae in §3 requires some discussion, after which results are presented which show that the blocking effect for $A \leqslant 1$ is similar to the linear case $A \to 0$. In §6 the more interesting case $A > 1$ is discussed.

The Fourier series (3.11) was truncated after $m = 10, 5, 3$ terms, depending (respectively) on whether $r/A < 1.1$, or $1.1 \leqslant r/A \leqslant 3.0$, or $r/A > 3$. This choice was checked by running the main numerical program with $\zeta_2 = -1$, and with the initial condition $L(x,0) = r_0(\theta)\sin\theta - 1$ (equation (4.1)), in which case the expected stationarity of $L(x,t)$ was obtained.

The V_0 component of the program utilizes a subroutine used and checked by the author in previous publications on the flow over straight boundaries.

The V_c component requires the largest computational time, since, in addition to a downstream integration, it requires a cross-stream integration (similar to that used by Stern & Whitehead 1990). This was accomplished by dividing the ordinate under each interfacial point into J equal parts, whose contributions to the cross-stream integral were summed using a trapezoidal approximation to the non-singular integrand for V_c. It was ascertained that the number of subdivisions used, viz. $J = 2 + \mathrm{Int}(10|L|)$, gave velocities insignificantly different from those obtained by tripling J. A test for coding errors was provided by formally setting $x' = \bar{x}$, $y' = \bar{y}$, in which case the V_c computer outputs from the double integration should be the same as the V_0 outputs (from a single contour integral) when both are evaluated at an x, y point lying slightly above the interface. The two numerical results differed by 1% which is the nominal design accuracy of the velocity calculations.

Initially the Lagrangian point separation was $\Delta x = 0.1$, and if the subsequent separation exceeded 0.15 a new Lagrangian point was inserted halfway in between. The y separation ΔL was also never allowed to exceed a specified amount ($\Delta L = 0.01$

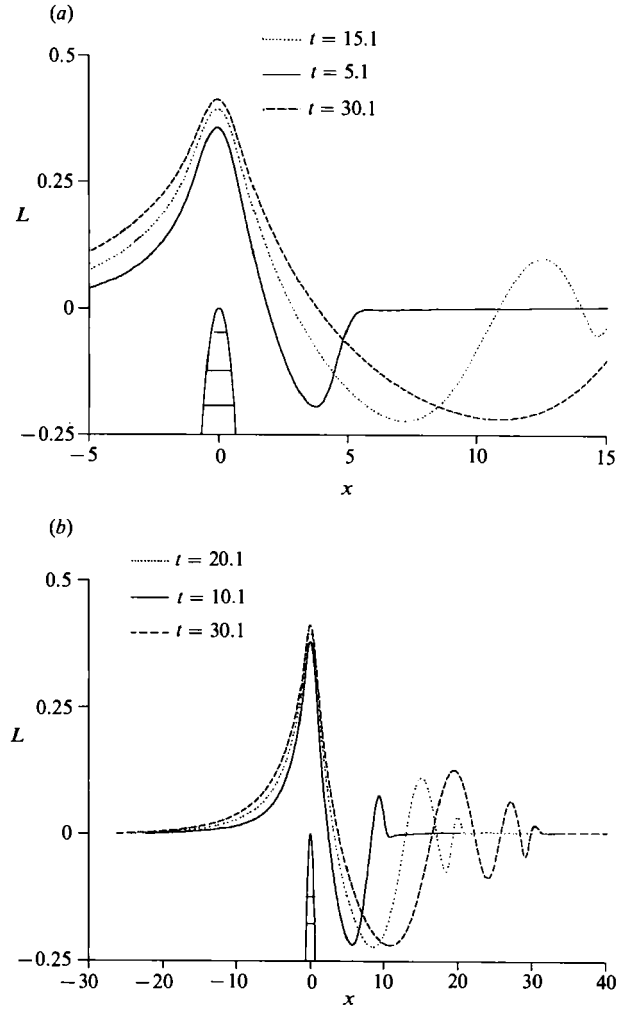

FIGURE 4(a, b). For caption see facing page.

for all the $A < 1$ calculations), and we also deleted neighbouring points when they came too close. A trapezoidal approximation to the downstream integration was made, and a second-order Runge–Kutta approximation with a time-step 0.1 was used. To prevent points from going through the rigid boundaries, no points were allowed to come closer than a small distance (0.05), but this precaution was only necessary for $A > 1$.

The left (minimum x) endpoint on the contour and the right endpoint were advanced with the undisturbed velocity (1, 0). A new left point was inserted behind the old one when its distance from a 'designated' point exceeded 0.15, and this point was moved slowly *upstream* to avoid endpoint contamination by the upstream propagating wave. When a new endpoint was inserted its L-value was not set exactly equal to zero (as would be appropriate if $x = -\infty$) but its (very small) value was determined by a linear extrapolation of the slope of L at the endpoint. This procedure avoided generating artificial 'kinks' in the curve which would have been propagated downstream into the main area of interest. Preliminary tests using *fixed* endpoints in

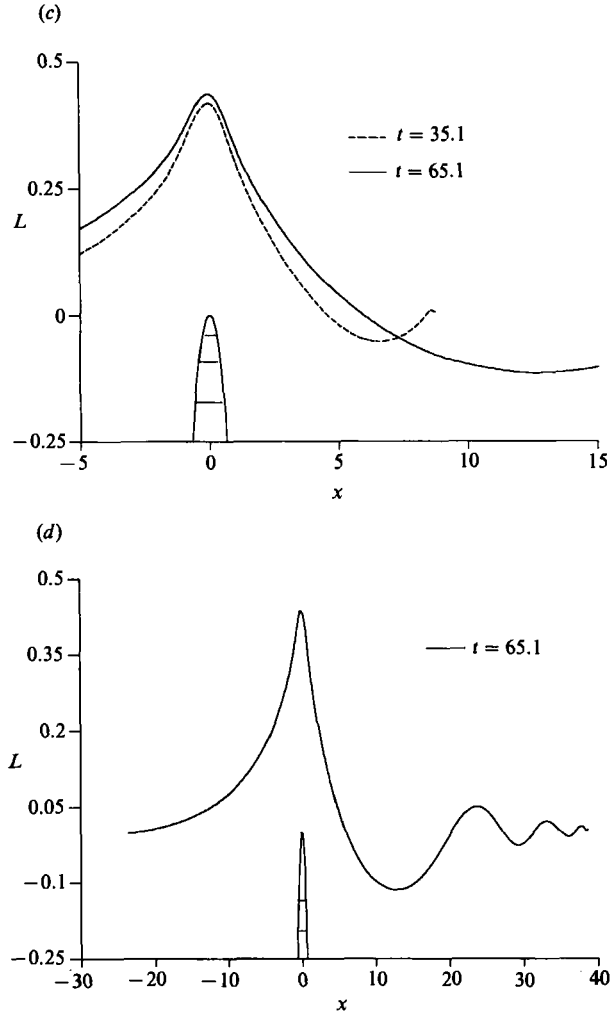

FIGURE 4. The solution of the contour dynamical equations when $\zeta_2 = 0$, $A = 1$, for the initial condition (5.1). Only the tip of the semicircular cape is shown. (*a*) A plot of a portion of L at three times showing the upstream ($x < 0$) propagation. (*b*) A full scale view of the same run. (*c*) The temporal continuation after 'truncating' (see text) a downstream portion of $t = 30.1$. (*d*) A full scale view of $t = 65.1$.

$-10 < x < 10$ showed a systematic drift in the total area bounded by L, but this error was greatly reduced by increasing the initial interval to $-20 < x < 10$, and by allowing the (right/left) endpoints to move (downstream/upstream) as indicated above.

Calculations were made for different values of (ζ_2, A) using an initial condition given by the solution of (4.1), viz.

$$L(x, 0) = r_0(\theta)\sin\theta - 1 \quad \text{with } A = 0.9, \tag{5.1}$$

and in some of the following calculations this was increased to

$$L(x, 0) = 2[r_0(\theta)\sin\theta - 1]. \tag{5.2}$$

Since the results of many runs for $A \leqslant 0.9$ were all qualitatively similar to the

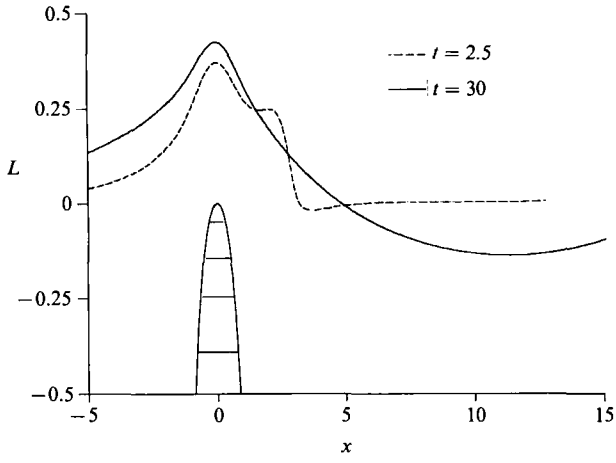

FIGURE 5. Same as figure 4(*a*) except that $L(x, 0)$ is twice as large.

$A = 1.0$ run, and quantitatively weaker in increasing the upstream area, only the $A = 1$ run will be discussed. The evolution of (5.1) with 300 initial Lagrangian points in $-20 < x < 10$ gave figure 4(*a*, *b*) for $L(x, t)$, and at $t = 30.1$ there were 730 points in $-26 < x < 40$. This evolution is qualitatively similar to the linear theory (figure 3*a*) even though A is not small. The increasing upstream area is compensated by the downstream trough in L, and figure 4(*b*) also shows the rapid downstream propagation of the short waves.

In order to concentrate on the further ($t > 30.1$) upstream development, a crucial assumption is now made to continue the calculation (with the computational resources available). It seems intuitively reasonable that anomalies far downstream from the cape will have a relatively minor influence far upstream, and therefore we truncated the downstream interface by setting $L = 0$ at all (Lagrangian) points succeeding one of the zero crossing points ($L = 0$), while leaving the upstream portion of the interface unaltered. This edited data then becomes a new 'initial' condition, and although the downstream evolution will obviously differ from an untruncated continuation, we believe that the truncation will only have a relatively small influence on the evolution upstream from the cape, and particularly on an integral property like (4.7). Evidence for the validity of this procedure will be presented.

When the $t = 30.1$ curve was truncated at the first zero-crossing ($x = 3.77$) the continuation yielded figures 4(*c*) and 4(*d*), and we note that at $t = 65.1$ the previously truncated downstream trough has been re-established. Of greater significance is the absence of any pronounced break at $t = 30.1$ when (4.7) is plotted as a function of $t^{\frac{1}{2}}$ (figure 6, solid points), and this continuity provides evidence that figure 6 would be the same even if no truncation had been made. For additional proof the calculation was repeated with $L(x, 0)$ doubled (i.e. (5.2) was used). This places some vortex anomalies so far above the cape that they tend to be 'blown' downstream, causing the ridge (figure 5) to collapse, generating a short wave which propagates downstream. The wave produces the 'knee' at $t = 2.5$, but afterwards ($t = 30$) the near-field evolution is similar to figure 4(*a*), and L at $x < 0$ continues to increase with time. At $t = 37.5$, L was again truncated at its first zero crossing ($x = 4.8$), and the calculation was then continued (not shown). The open squares (figure 6) for this run also show continuity and a near linear increase of upstream area with $t^{\frac{1}{2}}$. Since the asymptotic slope is nearly the same as the previous run, it is

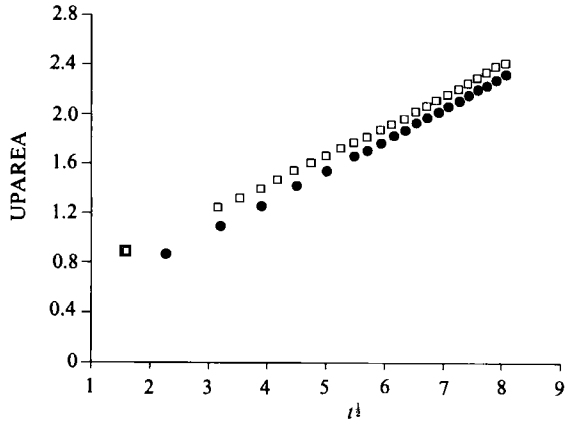

FIGURE 6. Plot of the integral of $L(x,t)$ from $x = -\infty$ to $x = 0$ for $A = 1$, $\zeta_2 = 0$. The solid points are for the run in figure 4, with a truncation at $t^{\frac{1}{2}} = 5.49$. The open points are for the run in figure 5 (different initial data), with a truncation at $t^{\frac{1}{2}} = 6.12$. No discontinuity at truncation is apparent in a curve which could be drawn through the points.

concluded that the upstream behaviour at $t \to \infty$ is independent of both the initial conditions and the downstream truncation. For $30 < t < 90$ the two slopes are approximately

$$\mathrm{d(UPAREA)}/\mathrm{d}t^{\frac{1}{2}} = 0.22 \quad (A = 1). \tag{5.3}$$

The velocities computed at $t = 30.1$ along the lower rigid boundary revealed an upstream minimum $u = -0.25$ at $x = -1.6$, $y = 0$. Stagnation points occurred on the cape at $x = -0.86$ and $x = 0.87$, and on $y = 0$ at $x = 4.3, 16.7, 22.4, 26, 29$. Such points are associated with closed streamlines, and the strongest of the downstream eddies (minimum $u = -0.21$ at $x = 1.4$) occurred in the immediate wake of the cape. On the upstream side of the cape a clockwise eddy forms as $\zeta = -1$ fluid near $y = 0$, $x = -A$ moves upstream, cross-stream, and then downstream to the forward stagnation point on the cape. But all of these eddies are thin in the cross-stream direction.

6. $A > 1$. Strong blocking

The modified V_s for this case (equations (3.13*a*, *b*)) was checked by computing the normal velocity at a point on the cape for $A = 2$. The magnitude was 5×10^{-3} when ten terms were retained in the Fourier series, and the magnitude decreased to 8×10^{-5} when the number of terms was increased to 50. The convergence of the series will be much more rapid for interfacial points which do not lie on the cape. The modified V_c and V_0 algorithms were tested in the same way as was done for the $A < 1$ case. The results of the $A > 1$ runs are as follows.

6.1. $A = 1.35$, $\zeta_2 = 0$

Using the same initial data (equation (5.2)) as in figure 5, figure 7 was obtained without truncation. Once again we see the development of a broad downstream trough ($L < 0$) induced by the clockwise vortices over the cape. The plot (not shown) of the upstream area

$$\mathrm{UPAREA} \equiv \int_{-\infty}^{0} (y_{\mathrm{L}}(x,t) - y_{\mathrm{b}}(x)\,\mathrm{d}x \tag{6.1}$$

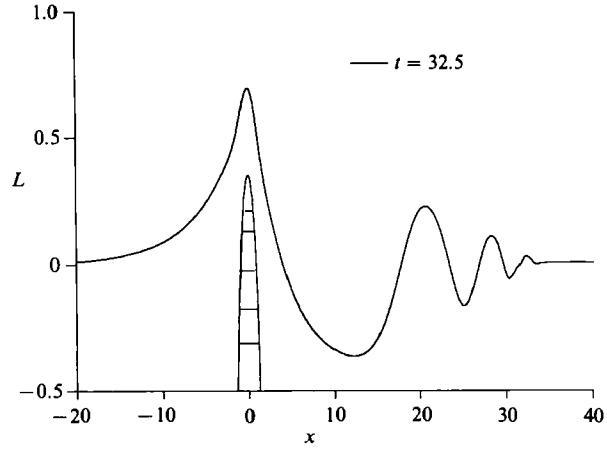

FIGURE 7. Plot of $L(x, 32.5)$ for $A = 1.35$, $\zeta_2 = 0$ with an initial $L(x, 0)$ identical to that used for figure 6.

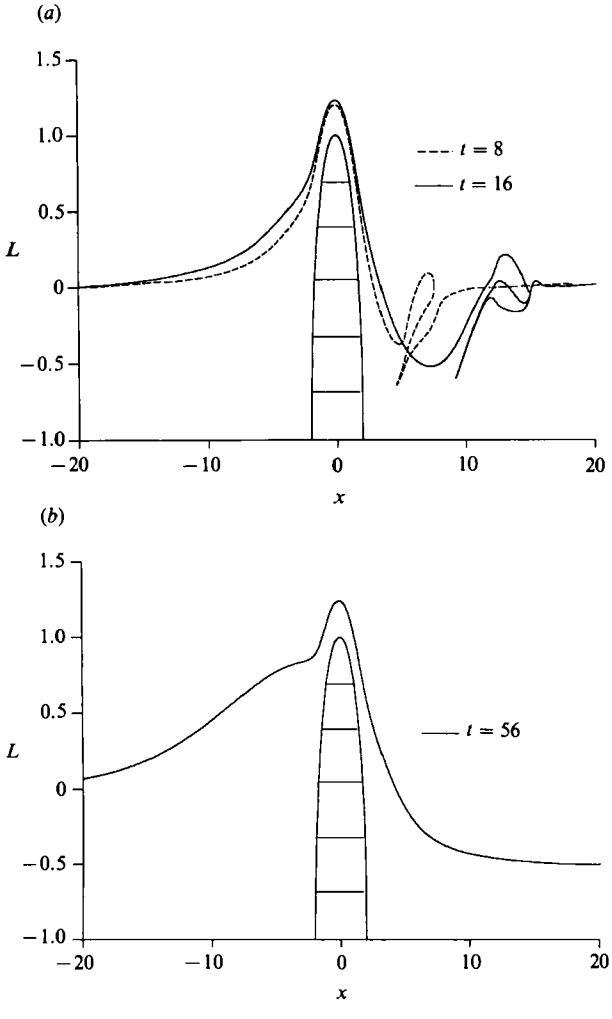

FIGURE 8(a, b). For caption see facing page.

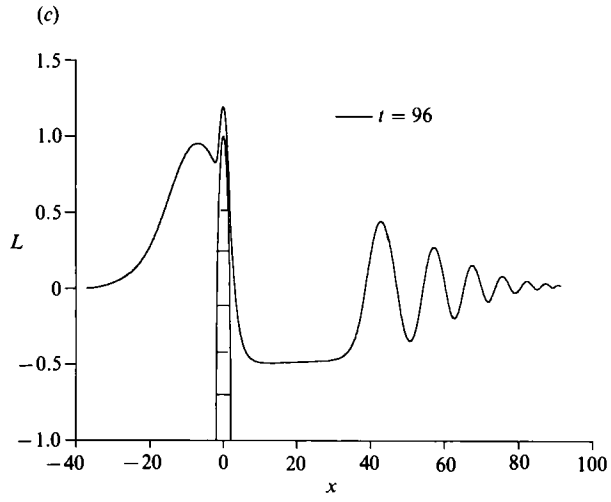

FIGURE 8. Plot of $L(x,t)$ for $\zeta_2 = 0$ and $A = 2$ using a larger $L(x,0)$ than in figure 7. (*a*) A small-scale ridge/trough system develops and propagates downstream until ($t = 16$) the ridge wraps around the trough, thereby surrounding irrotational fluid with $\zeta = -1$ fluid. (*b*) A continuation in which the $t = 16$ data was truncated by removing the small-scale plumes at large x. Note the inflection point in the region upstream of the cape at $t = 56$. (*c*) At $t = 96$ the inflection has developed into a minimum and a maximum. Note the tendency for the irrotational fluid to approach the wall ($y = 0$) downstream from the obstacle.

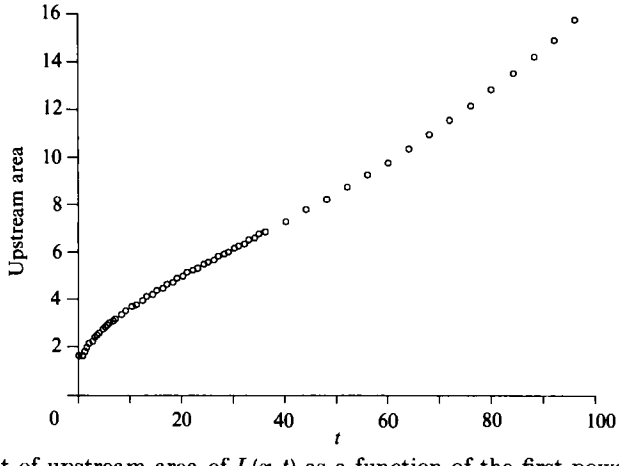

FIGURE 9. Plot of upstream area of $L(x,t)$ as a function of the first power of t for the whole time range of the figure 8 run ($A = 2$, $\zeta_2 = 0$).

for this case was similar to figure 6, and the rate is given by

$$\frac{\mathrm{d(UPAREA)}}{\mathrm{d}t^{\frac{1}{2}}} = 0.48,$$

or

$$\frac{\mathrm{d(UPAREA)}}{A^2\,\mathrm{d}t^{\frac{1}{2}}} = 0.26. \tag{6.2}$$

This normalized equation is also satisfied by the run pertaining to (5.3).

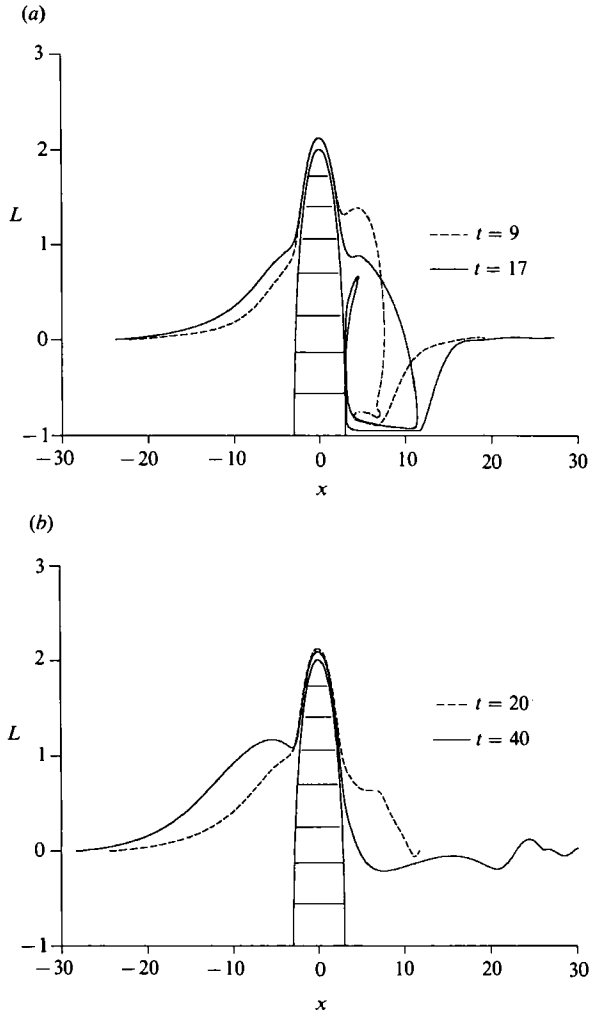

FIGURE 10(*a*, *b*). For caption see facing page.

6.2. $A = 2$, $\zeta_2 = 0$

To prevent the $t = 0$ interface from intersecting the cape we used an initial condition three times the value used for $A = 1.35$, so that $L(0, 0) = 1.46$, and thus the height of the ridge above the cape was 0.46. This distance is sufficiently large so that some of the vortex anomalies at the top of the cape are once again blown downstream, producing a secondary maximum L. At $t = 8$ (figure 8*a*) this secondary ridge appears as a thin plume containing clockwise vortices, and further downstream this induces the thin plume containing irrotational fluid. At $t = 16$ the latter is entrained in the $\zeta = -1$ layer. The plot (not shown) of UPAREA as a function of $t^{\frac{1}{2}}$ for this period gave

$$\frac{1}{A^2}\frac{\mathrm{d(UPAREA)}}{\mathrm{d}t^{\frac{1}{2}}} = 0.24 \quad (4 < t < 16), \tag{6.3}$$

which is the same as (6.2) (but the absolute rate $(0.24A^2)$ in this case is four times larger). The calculation was continued in time after truncating the $t = 16$ output so

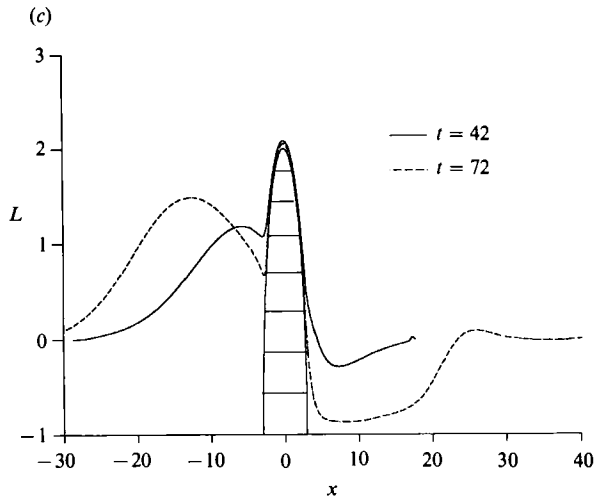

FIGURE 10. Larger amplitude than in figure 9: $A = 3$, $\zeta_2 = 0$. $L(x,0) = 2.5/(1+(x/A)^4$. (*a*) The $L(x,t)$ curves show the development of a large clockwise eddy in the wake of the cape. At $t = 9$ and $x \sim 5$ the large upstream velocity near the wall produces the filament of irrotational fluid which approaches the base of the cape, and then ($t = 17$) rises. (*b*) Continuation of figure 10(*a*) obtained by truncating its downstream part at $t = 19$ (compare $t = 20$ with $t = 17$). At $t = 40$ there is no change in L over the cape, but there is a large increase in upstream area accompanied by a maximum and a minimum L. (*c*) A continuation of figure 10(*b*) obtained by truncating the $t = 40$ result beyond $x = 15.5$ ($L = -0.05$) and smoothing L to zero. The result is shown a short time later ($t = 42$), and later ($t = 72$) the minimum upstream $L = 0.67$ (at $x = -2.7$) has decreased considerably due to the downward velocities induced by the large amount of anti-cyclonic vorticity further upstream. Also note the nearly complete attachment of the irrotational free stream to the downstream wall. This diagram shows that essentially none of the vortical fluid in the upstream boundary layer passes around the cape.

as to remove all Lagrangian points beyond the second zero crossing point (figure 8*a*), which occurs at the relatively large value of $x = 11.5$. The 'new initial condition' then consisted of a single-valued L having a ridge over the cape and one complete trough downstream. Forty time units later (figure 8*b*) $L(x,t)$ is still increasing at $x < 0$, and a 'knee' (the broad inflected region) appears. The region upstream from this is sufficiently far from the cape, and L is sufficiently large, so that a pronounced free wave steepening effect (according to (2.14)) may be expected at larger t, and we also expect that the accumulating upstream vorticity anomalies will induce downward velocities on the cape ($x < 0$). Both of these expectations are confirmed in figure 8(*c*), where the inflected knee has evolved into a maximum and a minimum. The downward v-motion at and below this minimum L indicates a strong blocking of the approaching boundary-layer flow. This is confirmed (figure 9) by plotting UPAREA against the first power of t. The '$t^{\frac{1}{2}}$-regime' of early times ($t < 12$) gives way to a 't^1-regime', implying that a constant fraction of the boundary-layer flux from $x = -\infty$ is recirculated upstream by the blocking. Although no truncation after $t = 16$ was made we see (figure 9) that at $t = 61$ the upstream area starts to increase even more rapidly, at the same time as the inflected region (figure 8*b*) develops into the minimax region (figure 8*c*). The development of the upstream minimum L, with the associated negative v, is a clear indication that the increase in upstream area (figure 9 at large t) is not due to a small systematic and cumulative numerical error. Figure 8(*c*) also shows that the interface behind the cape plunges towards the wall ($y = 0, L = -1$) indicating a tendency for the free stream ($\zeta_2 = 0$) to reattach.

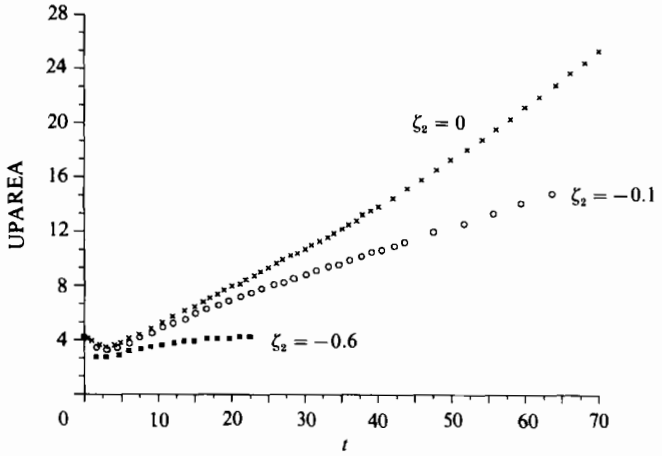

FIGURE 11. Plot of upstream area *vs.* time for $A = 3$, and various ζ_2. See figures 12 and 13 below.

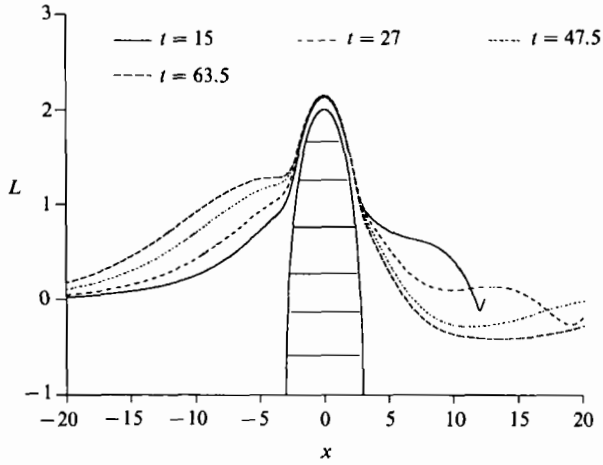

FIGURE 12. Same as figure 10 except $\zeta_2 = -0.1$ showing that a small amount of boundary-layer fluid now passes around the cape.

6.3. $A = 3$, $\zeta_2 = 0$

To avoid intersection with the cape, a further increase in the initial amplitude is required, and (for the first time) the interfacial shape was also changed to

$$L(x,0) = \frac{2.5}{1+(x/A)^4}.$$

The initial distance (0.5) of the L-ridge above the cape is approximately the same as in the previous run, and the evolution (figure 10*a*, *b*) is qualitatively similar but quantitatively more extreme. The clockwise vortices blown downstream accumulate at $t = 17$ in a large clockwise wake eddy, whose base lies on $y = 0$. This evolved from the $t = 9$ flow as the thin plume of irrotational fluid wound clockwise along $y = 0$, and then rose to almost detach a $\zeta = -1$ eddy. At $t = 19$ (not shown) there is a large upstream velocity $u = -0.53$ at the base ($x = 5.4$) of this eddy, and at ($x = 3.01$, $L = -0.4$) there is a large positive $v = 0.31$. Thus almost all of the boundary layer

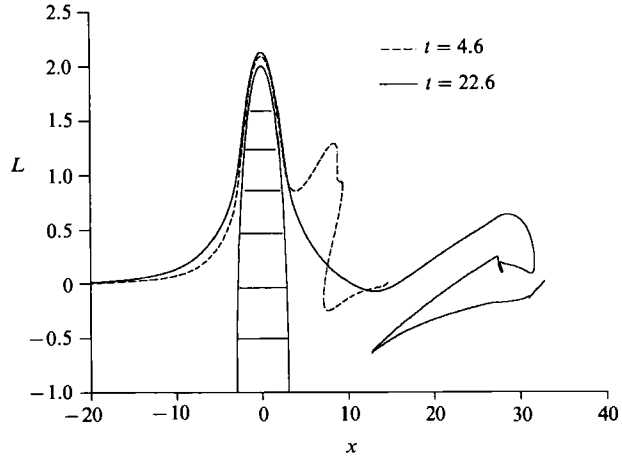

FIGURE 13. Same as figure 12 except $\zeta_2 = -0.6$ (no data truncation). The initial ridge at $x = 0$ propagates rapidly downstream as a secondary ridge. The ridge velocity $u(0, 22.6) = 3.6$ is sufficient to transport almost all of the boundary layer downstream.

flowing around the cape goes into the wake vortex. Further downstream ($x = 13$, $y = 0.05$) on the wall (at $t = 19$) there is a large downstream wall velocity $u = 0.71$, indicating that the downstream boundary layer is being pushed away by the 'reattaching' free-stream of irrotational fluid. We are unable to pursue these extremely interesting downstream effects (will the wake eddy by permanently trapped?) further in time because of the large number of Lagrangian points, because a proper 'surgerizing' algorithm (Dritschel 1988) is required, and because we decided to focus on the upstream effect. Consequently $L(x, 19)$ was truncated beyond the first zero-crossing ($L = 0$) at $x = 10.3$, and the continuation with this new initial condition is shown in figure 10(*b*, *c*). The slight upstream knee inflection at $t = 20$ again develops ($t = 40$) into a more pronounced minimax. The interfacial point $L(0, 72) = 2.05$ is essentially on the cape since the numerical program does not allow the distance of Lagrangian points from the cape to be less than 0.05. The same is true for all points $-2.47 < x < 1.16$, and at $x = -0.27$ the minimum L has a small negative v. Thus we see that at $t = 72$ essentially none of the $\zeta_2 = -1$ layer fluid is flowing around the cape, and all of this fluid is accumulating in a large clockwise vortex lying upstream from the cape. This complete blocking of the boundary layer is also implied by the temporally increasing rate of change of the upstream area, as indicated by the $\zeta_2 = 0$ points in figure 11. If there is any break or discontinuity at the truncation times ($t = 19$ and $t = 40$) it is no larger than the irregularity of adjacent points between these times, and thus a smooth curve could be drawn through all points, thereby supporting the assumption that the increase in the upstream area is negligibly affected by the truncation.

6.4. *Decreasing ζ_2 with $A = 3$*

We then decreased the upper-layer vorticity to $\zeta_2 = -0.1$ (other things being equal) in order to show that blocking can occur for large L even when infinitesimal amplitude long waves propagate downstream (cf. (2.14)).

The initial evolution for $\zeta_2 = -0.1$, $A = 3$ was similar to that in §6.3 insofar as a large clockwise wake eddy formed, but its size was smaller. For example, at $t = 13$ (not shown) the minimum distance of the interface from the wall was $y = 0.08$, as

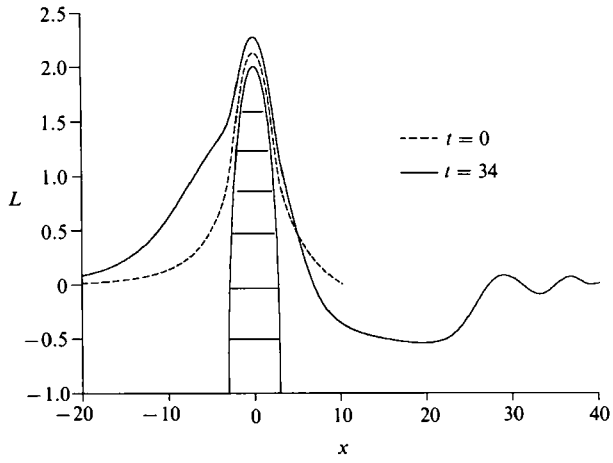

FIGURE 14. The undisturbed velocity at $y \geqslant 0$ has been increased by $W = 0.25$. $A = 3$, $\zeta_2 = 0$. This initial condition yields a finite blocking fraction (see text), but for a larger $W = 1.5$ there was no blocking.

compared to $y = 0.05$ when $\zeta_2 = 0$. Also, as in figure 10(a), a thin intrusion of irrotational fluid near $y = 0$ in the lee of the cape moved upstream and wound clockwise around the wake eddy. The $t = 13$ output was then truncated beyond the first zero crossing, and the run was continued uninterruptedly to $t = 63.5$. Figure 12 shows the upstream propagation leading to the same kind of inflection point (a 'knee') at $L(-4, 63.5)$ where v has a minimum ($+8 \times 10^{-3}$) nearly equal to zero. At $x = 0$ the maximum $L\,(= 2.15)$ is now at a significant distance (0.15) above the top of the cap, and the large velocity $u(0, 63.5) = 2.0$ enables a finite fraction of the wall layer ($\zeta = -1.0$) to flow around the cape. This can be seen from the slope of the curve connecting the $\zeta_2 = -0.1$ points in figure 11. The decreased slope of the $\zeta_2 = -0.1$ curve (figure 11), compared to $\zeta_2 = 0$, combined with the steady solution for $\zeta_2 \to -1$ suggests that there is a critical $\zeta_2 < 0$ above which the rate of increase of upstream area is greater than zero when $t \to \infty$. An estimate of the critical ζ_2 can be obtained from (2.16), and for $A = 3$, the approximate ζ_2 is -0.4. Therefore, we set $\zeta_2 = -0.6$ [keeping everything else the same as in the $\zeta_2 = -0.1$ run (figure 12)] expecting that the blocking should vanish at large t. The reduced vorticity anomalies in this case cause a large fraction of the ridge (figure 13) to be rapidly blown downstream, after which $L(x, t)$ appears to be approaching a steady symmetrical distribution about $x = 0$ (at least for $x < 10$). Further evidence for vanishing blocking is supplied by the plotted $\zeta_2 = -0.6$ points (figure 11), which indicate that the rate of increase of upstream area rapidly approaches zero. Therefore the critical ζ_2 lies between -0.6 and -0.1, and is in rough agreement with the theoretical estimate $\zeta_2 = -0.4$.

The general inference from this calculation is that even for large obstacles there is a critical cross-stream distribution of undisturbed vorticity for which no upstream influence (and no modification of the source region) occurs. Otherwise such a large obstacle may modify the upstream vorticity distribution so as to bring about a new state satisfying this critical condition.

Further evidence for this conclusion was obtained by adding a uniform downstream velocity W at $x = -\infty$. Since this increases the downstream propagation of all waves, a sufficiently large W should also remove the blocking effect obtained (figure 10) for $\zeta_2 = 0$, $A = 3$. In order to expedite this new calculation, a convenient

initial condition was used which eliminates the large wake vortex found in the previous ($A = 3$) calculations. Accordingly, the last output from the $\zeta_2 = -0.1$, $A = 3$ run was truncated to obtain the $L(x, 0)$ shown in figure 14. The evolution of this for $W = 0.25$ gave

$$\mathrm{d(UPAREA)}/\mathrm{d}t = 0.19 \pm 0.005 \quad (10 < t < 20),$$

but when W was increased to 1.5 (keeping everything else the same), the rate of increase of upstream area (5×10^{-4}) at $t = 16$ was essentially zero. Thus there is a critical W (between 0.25 and 1.5), such that all influences are propagated downstream, and no blocking occurs.

7. Conclusion

A large obstacle placed in the 'boundary layer' of an inviscid flow can produce an upstream influence, which blocks the boundary layer and accumulates vorticity in a large upstream eddy.

Although finite Reynolds number flow is beyond our scope, it is worth noting that the accumulation of vorticity in such eddies is observed (e.g. p. 35 of Schlichting 1968) when a blunt obstacle is placed at some distance downstream from the leading edge of a flat plate (Blausius flow). The resulting upstream regime is very different from that which occurs when either the plate is removed from the obstacle, or the obstacle is removed from the plate. It is suggested that the purely inertial effect studied herein is relevant to the establishment of the upstream eddy when the boundary plate is present.

The flow downstream from the obstacle (figure 10*a*) is also drastically modified, but the computational technique used to study the upstream effect has not allowed an adequate investigation of the wake field.

In classical open channel hydraulics, blocking of a uniform stream does not occur when long waves are capable of propagating upstream from an obstacle, and it is therefore noteworthy that blocking only occurs in our barotropic shear flow when long waves can propagate upstream. The role of barotropic shear as well as gravity effects should be taken into account in determining the controlling effect of ocean straits and topography on large-scale currents, and in producing upstream or downstream transitions in the flow past coastal irregularities.

REFERENCES

Dritchel, D. G. 1988 The repeated filamentation of vorticity interfaces. *J. Fluid Mech.* **191**, 511–517.

Gill, A. E. 1977 The hydraulics of rotating channel flow. *J. Fluid Mech.* **80**, 641–671.

Higdon, J. J. L. 1985 Stokes flow in arbitrary two-dimensional domains. *J. Fluid Mech.* **159**, 195–226.

Hughes, R. L. 1986 On the conjugate behavior of weak along-shore flows. *Tellus* **38** A, 277–284.

Hughes, R. L. 1987 The role of higher shelf modes in coastal hydraulics. *J. Mar. Res.* **45**, 33–58.

Pratt, L. J. & Armi, L. 1987 Hydraulic control of flows with nonuniform potential vorticity. *J. Phys. Oceanogr.* **17**, 2016–2029.

Schlichting, H. 1968 *Boundary Layer Theory*. McGraw Hill.

Stern, M. E. 1972 Hydraulically critical rotating flow. *Phys. Fluids* **15**, 2062–2064.

Stern, M. E. 1975 *Ocean Circulation Physics*. Academic.

Stern, M. E. & Paldor, N. 1983 Large amplitude long waves in a shear flow. *Phys. Fluids* **26**, 906–919.

STERN, M. E. & PRATT, L. J. 1985 Dynamics of vorticity fronts. *J. Fluid Mech.* **161**, 513.

STERN, M. E. & WHITEHEAD, J. 1990 Separation of a boundary jet in a rotating fluid. *J. Fluid Mech.* **217**, 41–69.

TURNER, J. S. 1973 *Buoyancy Effects in Fluids*. Cambridge University Press.

WHITEHEAD, J. A., LEETMA, A. & KNOX, R. A. 1974 Rotating hydraulics of strait and sill flows. *Geophys. Fluid Dyn.* **6**, 101–125.